Optimal Thickness of a Porous Micro-Electrode Operating a Single Redox Reaction

Tien Dung Le, Lin Zhang, Stephane Reculusa, Gérard Vignoles, Nicolas Mano, Alexander Kuhn, Didier Lasseux

ChemElectroChem **2019**, *6*, 173 – 180 - DOI: 10.1002/celc.201800972

Optimal Thickness of a Porous Micro-Electrode Operating a Single Redox Reaction

Tien D. Le,[a] Lin Zhang,[b, d] Stéphane Reculusa,[b] Gérard Vignoles,[c] Nicolas Mano,[d] Alexander Kuhn,[b] and Didier Lasseux*[a]

This article reports on a procedure to predict the optimal thickness of cylindrical porous electrodes operating a single redox reaction. This is obtained from a macroscopic model for the coupled diffusion-reaction process that is first validated with voltammetry experiments of the H_2O_2/H_2O reduction reaction carried out with a series of porous electrodes elaborated in this work. An analytical solution to this model is developed in the steady regime and for electrodes featuring a thickness to mean radius ratio small enough compared to unity. An analytical expression of the optimal electrode thickness is derived corresponding to the crossover value of two asymptotic regimes characterizing the dependence of the volume current density produced by the electrode upon its thickness. The predictive tool of the optimal thickness is general, regardless of the porous microstructure. The case of the electrodes used in the reported experiments illustrates that the optimal thickness is not intrinsic to the microsctructure characterized by the size of the representative volume, its specific area and effective diffusion coefficient. It also depends on the operating conditions reflected in the kinetic number, *Ki*, and the thickness of the diffusion layer surrounding the electrode. The dependence of the optimal thickness on these two parameters is quite significant in a range of very small values of *Ki* but remains quasi constant beyond a threshold value.

1. Introduction

In the recent past decades, porous electrodes, which are of major interest for the design of miniaturized electro-devices such as bio-batteries or bio-sensors, have recieved considerable attention both from modeling and experimental points of view.[1–8] A well-defined pore size and pore distribution of the porous material may be achieved by using the Langmuir-Blodgett templating technique,[9–11] providing a high surface-to-volume ratio (specific area).[9,12] Such a feature allows the electrodes to produce much higher electrical current per unit volume than classical flat electrodes of the same macroscopic size.[11] In addition, the overall thickness of the electrode may be well-controlled during the elaboration process with an accuracy of about 10 nm.[13] However, prediction of the optimal electrode thickness, yielding the best compromise between an optimal electricity production and an economical manufacturing, is still an open question. Intuitively, it can be easily understood that the process of diffusion coupled to electrochemical reaction, supplied by the external fluid layer containing the reactant and in contact with the porous electrode, is becoming less effective in the core of the electrode, far from the interface with this fluid layer, as a result of reactant depletion. This calls upon a specific analysis, based on a rational physical modeling, in order to determine the optimal thickness compatible with this cut-off mechanism.

Modeling of the macroscopic behavior of a porous electrode has received much attention in the literature.[14,15] In more details, the coupled diffusion-reaction mechanisms within the porous medium have been addressed in different regimes including the Direct Electron Transfer mode[2,16] or Mediated Electron Transfer regime.[3,17] An empirical macroscopic model was developed for a porous electrode composed of spherical pores deposited on a disk under the assumption that the process can be treated as if all the pores are behaving independently from each others.[18] During almost the same period, a pore-scale modeling of diffusion-reaction in a porous electrode, composed of parallel cylindrical solid protrusions deposited on an electrode surface, was presented together with direct numerical simulations in order to analyse different electrochemical scenarii of reversible and irreversible electron transfer processes.[19,20] An empirical analytical macroscale model for transport and reaction in an infinite porous rotating disk electrode was also developed in the convection- and diffusion-dominated regimes.[21,22] On a more formal basis, an upscaling procedure was applied to a coupled transport-reaction problem at play in a porous electrode containing three phases (solid, liquid and gas) yielding governing equations at the macroscale.[23] However, the macroscale model remains unclosed as no closure was provided to estimate the effective parameters. Recently, a rational upscaling procedure was

[a] *Dr. T. D. Le, Dr. D. Lasseux*
Institut de Mécanique et d'Ingénierie, CNRS, UMR5295 Esplanade des Arts et Métiers, 33405 Talence, France
E-mail: didier.lasseux@u-bordeaux.fr
[b] *Dr. L. Zhang, Dr. S. Reculusa, Prof. A. Kuhn*
University of Bordeaux, CNRS UMR5255 Bordeaux INP, Site ENSCBP, 16 Avenue Pey Berland 33607 Pessac, France
[c] *Prof. G. Vignoles*
Laboratoire des Composites ThermoStructuraux, CNRS, UMR5801 3 Allée de la Boétie, 33600 Pessac, France
[d] *Dr. L. Zhang, Dr. N. Mano*
Centre de Recherche Paul Pascal, CNRS, UMR5031 Avenue Albert Schweitzer, 33600 Pessac, France
An invited contribution to a Special Issue in celebration of our 5 Year Anniversary

applied to the initial boundary value problem governing the coupled diffusion-reaction process at the pore-scale to obtain the macroscopic model and the ancillary closure problem providing the effective diffusivity.[24] Such an approach is capable of capturing the microstructure properties of the electrode and its influences on the effective parameters at the macroscale. The macroscopic model obtained was validated by comparison with 3D-Direct Numerical Simulations (DNS) of the pore-scale model as well as with experimental data involving the reduction reaction of oxygen to hydrogen peroxide.[24]

Although considerable progress has been made for porous electrode manufacturing and electrochemical characterization of the material, an empirical approach toward a systematic prediction of an optimal design, in particular in terms of the best effective electrode thickness, is not sufficient. Optimal electrode thickness for a plane solid oxide fuel cell was discussed in a work by Cai et al.[25] based on 3D direct simulations at the pore-scale. Results for the optimal thickness were obtained, indeed, on an empirical basis by performing repeated simulations on a series of electrodes with different thicknesses, yielding a conclusion very specific to the case under study. In fact, no general formulation was proposed to predict such an optimal thickness and the relevant reduced parameters on which it depends were not highlighted while operating conditions (temperature, reaction rates, electron and ion transfer processes) were quite different from those considered in the present work. To the best of our knowledge, no alternative approach has been followed in the literature towards this goal. The present work aims at a progress to fill this gap by developing a thorough approach to estimate the optimal thickness of a porous electrode operating with a single redox reaction using the macroscopic model formally derived in a previous work.[24]

The article is organized as follows. The upscaled formal model operating at the macroscale[24] is first briefly recalled and its solution is compared to a series of experimental results of hydrogen peroxide reduction to water, carried out in this work, with the purpose of an additional further validation. Secondly, this macroscopic model is used in the steady-state regime (a situation which is of wide practical interest) to derive an analytical model for the concentration profile of the dilute species allowing to express the current intensity available at the electrode. On this basis, an optimization procedure is finally proposed to estimate the effective electrode thickness. This yields an analytical expression of the optimal thickness that is general for a cylindrical porous electrode, regardless the type of microstructure of the electrode material. An illustration is provided for the type of electrode used in the experiments reported in this work.

2. Multiscale Diffusion-Reaction Model in a Porous Electrode

In this section, the multiscale model developed in a previous work[24] for a diffusion and electrochemical reaction problem within a porous micro-electrode is briefly recalled. It consists in a bottom-up approach which allows to take into account the microstructural information together with the physics of diffusion and reaction within the porous medium in order to obtain a reduced model that retains the essential features of the process at the underlying scale. In essence, this is achieved by applying the volume averaging method[26] to upscale the pore-scale initial and boundary value problem yielding a macroscopic model operating at the electrode scale.

At the pore scale, a single reduction reaction at the solid-fluid interface within the porous cathode is taken into account, namely

$$A + ne^- \xrightarrow{k_0} B \qquad \mathbf{r} \in I_{sf} \tag{1}$$

where I_{sf} is the fluid-solid interface, $\mathbf{r}$ the position vector at I_{sf}, n and k_0 the number of electrons transferred and the electron transfer rate constant, respectively. The redox couple A/B experiences a simple reduction reaction such as O_2/H_2O_2, H_2O_2/H_2O, etc. Letting c_A and D_A be the concentration and diffusion coefficient of species A in the pores within the electrode occupying a domain Ω, the mass transfer of species A, diluted in the fluid in which the electrode is immersed, is governed by Fick's law[27] and the overall process can be described by the following initial and boundary value problem

$$\frac{\partial c_A}{\partial t} = \boldsymbol{\nabla} \cdot (D_A \boldsymbol{\nabla} c_A) \quad \text{in } \Omega_f \subset \Omega \tag{2a}$$

$$\text{B.C.1} \quad -\mathbf{n} \cdot D_A \boldsymbol{\nabla} c_A = k_0 \exp\left(\frac{-\alpha n F (E - E^0)}{RT}\right) c_A \quad \text{at } I_{sf} \tag{2b}$$

$$\text{B.C.2} \quad c_A = G_A(\mathrm{r}, t) \quad \mathrm{r} \in A_{fe},\ \forall\ \mathrm{t} \tag{2c}$$

$$\text{I.C.} \quad c_A = F_A(\mathrm{r}) \quad \mathrm{r} \in \Omega_f,\ \mathrm{t} = 0 \tag{2d}$$

Here, α, E and E_0 are the electron transfer coefficient, electrode potential and standard potential respectively, $\mathbf{n}$, F, R and T the normal unit vector at the fluid solid interface pointing out of the fluid phase, Faraday constant, ideal gas constant and temperature. It should be noted that the interfacial condition B.C.1 is based on the Butler-Volmer equation which provides a relationship between the current density and the concentration.[28] In addition, in boundary condition B.C.2, $A_{fe} = \Omega_f \cap \Omega_e$ is the entrance and/or exit boundary of the fluid domain, Ω_f, from/into the diffusion layer, Ω_e, at the external boundary of the electrode in contact with the bulk fluid.

For a given microstructure, a DNS of the above problem can be performed[24] however to the cost of a very demanding solution in terms of computational time and memory resources. Alternatively, an upscaling procedure, based on the volume averaging method can be employed to derive a macroscopic model that may lead to a 1D simulation for a plane or circular electrode and uniform boundary conditions for instance. Let $\langle c_A \rangle^f$ be the average concentration in the fluid phase defined by

$$\langle c_A \rangle^f = \frac{1}{V_f} \int_{V_f} c_A dV \tag{3}$$

where V_f (of measure V_f) denotes the portion of the averaging volume occupied by the fluid phase. The upscaling procedure yields the following macroscopic mass conservation equation

$$\varepsilon_f \frac{\partial \langle c_A \rangle^f}{\partial t} = \nabla \cdot \left(\varepsilon_f \mathbf{D}_{eff} \cdot \nabla \langle c_A \rangle^f \right) - k_0 \exp\left(\frac{-\alpha n F (E - E^0)}{RT} \right) a_v \langle c_A \rangle^f \tag{4}$$

In this equation, ε_f and a_v are the porosity and specific area respectively; $\mathbf{D}_{eff}$ is the effective diffusion tensor given by

$$\mathbf{D}_{eff} = D_A \left(\mathbf{I} + \frac{1}{V_f} \int_{A_{sf}} \mathbf{n}\mathbf{b} \mathrm{dA} \right) \tag{5}$$

where **b** is the closure variable vector field relating the local concentration to the gradient of its average and is solution of an intrinsic closure problem on a representative elementary volume of the porous electrode (see Eqs. (16) in Le *et al.*[24]). In Eq. (5), **I** and A_{sf} are denoting the identity tensor and the solid/fluid interface in the averaging volume.

The macroscale diffusion-reaction Equation (4) is obtained under the constraint that the process at the pore-scale occurs in the mass-transfer limited regime, i.e., that the pore-kinetic (or pore-Damköhler) number, Ki_p, which represents the reaction rate to diffusion rate ratio (or the ratio between the characteristic time associated to diffusion and the characteristic time associated to reaction at the pore-scale) remains much smaller than unity.[26,29] This is expressed as

$$Ki_p = k_0 \exp\left(\frac{-\alpha n F (E - E^0)}{RT} \right) \ell_p / D_A \ll 1 \tag{6}$$

ℓ_p being the characteristic pore size, a constraint which is easily met in practice. The form of Eq. (4) and stationarity of the closure problem on **b** are also subject to a constraint on the time scale given by $\frac{D_A t}{\ell_p^2} \gg 1$. This indicates that the overall process must be observed at a time larger than the characteristic time for difussion at the pore-scale.[26]

Subsequently, the macroscopic mass transfer Equation (4) may be solved together with Fick's law in the external diffusion layer and appropriate macroscopic boundary and initial conditions, to obtain the macroscopic concentration profile of species *A* inside the porous electrode at any time. This field can then be used to compute the total current intensity delivered by the electrode that is given by (see Le et al.[24] for the details)

$$I = -n k_0 F \exp\left(\frac{-\alpha n \, F (E - E^0)}{RT} \right) a_v \int_{\Omega} \langle c_A \rangle^f \mathrm{d}V \tag{7}$$

At this stage, it must be noted that the macroscopic model is very general as it does not make any assumption neither on the internal microscopic structure (provided a representative elementary volume can be extracted) nor on the macroscopic shape of the entire electrode.

Concentration profiles and current intensity obtained from this macroscopic approach were compared to results of 3D DNS of the pore scale model for a cylindrical porous electrode, showing an excellent agreement between the two,[24] with, however an enormous solution speed-up achieved with the 1D macroscopic approach.

3. Application of the Macroscopic Model

Before using the macroscopic model to estimate the optimal thickness of a cylindrical electrode in a general case, a comparison with results of H_2O_2/H_2O reduction experiments performed on microporous electrodes is first carried out for further validation purposes. It must be emphasized that the experimental conditions are kept the same for the simulations of the macroscopic model.

3.1 Comparison with Experimental Data

Five porous gold-coated electrodes made of 5, 7, 11, 15 and 19 half-layers (*HL*) of pores were manufactured according to a three-step procedure.[10] An organized colloidal template of silica beads of diameter $d_s = \ell_p = 1.17$ μm was first deposited on a gold wire of radius $R_1 = 125$ μm, using the Langmuir-Blodgett technique and controlling the number of bead layers.[13,30] It should be noted that two half-layers correspond to one silica bead layer in the electrode manufacturing process. In a second step, gold was electrodeposited in the space between the beads before their dissolution in a third and final step. This yields a spherical pore network close to a FCC structure with a pore connection window of diameter d_c, resulting from the limitation of gold deposition. The connection window size was estimated to be $d_c = 0.15 d_s \cong 0.176$ μm, a value that can be considered as the minimum value for this type of manufacturing process for these electrodes.[31] Given these values for d_s and d_c and adopting a FCC structure, all other structural parameters can be deduced, namely the porosity $\varepsilon_f = 0.763$, the specific area $a_v = 3.567 \times 10^6$ m^{-1} and the size of the geometrical periodic unit cell, corresponding to 4*HL*, $\ell_R = 1.64$ μm (see Figure 1).

Electrodes were then immersed in a 0.5 M H_2SO_4 solution containing dissolved 10 mM hydrogen peroxide (species *A*). Voltammetry experiments were carried out at a temperature $T = 298$ K and a scan rate $r_E = 0.5$ mV/s, decreasing the potential from 0.5 V to 0 V in order to observe the reduction of hydrogen peroxide to water. The active surface area, S_{act}, for the 5*HL*, 7*HL*, 11*HL*, 15*HL* and 19*HL* electrodes, measured during the experiments, are 1.63, 2.23, 3.5, 5 and 6.3 cm^2 respectively which were used for the numerical simulations.

To avoid a simplification which would consist in considering the electrodes used in the experiments as quasi-planar (this approximation will be considered latter in this article), the macroscale model is solved in a 2D cross section as represented

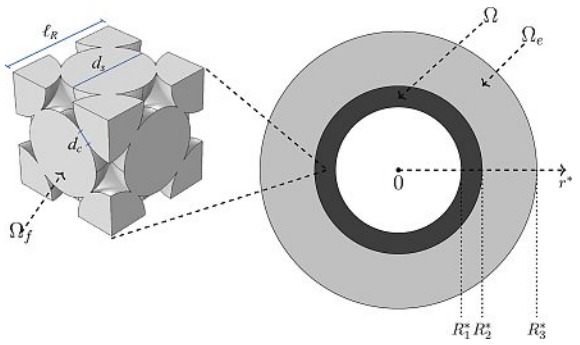

Figure 1. Configuration of the 2D-computational domain and FCC model microstructure composing the electrode material.

in Figure 1, yielding a rotationally symmetrical 1D radial problem. By doing so, it is assumed that no significant effects are induced by the electrode extremities in the axial direction. For convenience, the problem is expressed in a dimensionless form in which the dimensionless concentration, radial coordinate and time, denoted with the superscript *, are respectively normalized by the initial concentration of hydrogen peroxide, c_A^0, the unit cell size of the FCC structure described above, ℓ_R, and the characteristic time for diffusion, ℓ_R^2/D_A. In the configuration presented in Figure 1, $r^* = 0$ locates the gold wire axis, $r^* = R_1^*$ is the dimensionless gold wire radius while the electrode, of normalized thickness L_e^*, occupies the region $R_1^* \le r^* \le R_2^* = R_1^* + L_e^*$, of section $S^* = S/\ell_R^2$, where the macroscopic mass balance Equation (4) applies. Note that if N_h is the number of half layers composing the electrode, $L_e^* = N_h/4$, taking into account the FCC model structure. In the bulk fluid surrounding the electrode, the dimensionless diffusion layer, of normalized thickness L_N^*, is present at $R_2^* \le r^* \le R_3^* = R_1^* + L_e^* + L_N^*$ where mass transport is governed by Fick's law (see Eq. (2a)). At the gold wire/electrode interface ($r^* = R_1^*$) a no flux condition is applied, while at the electrode/diffusion layer interface ($r^* = R_2^*$), continuity of the concentration and flux are imposed and, at the external boundary of the diffusion layer with the rest of the bulk fluid, a Dirichlet boundary condition is considered, i.e., the H_2O_2 concentration remains equal to c_A^0. As a consequence, the boundary value problem describing the process can be stated as follows

$$\varepsilon_f \frac{\partial \langle c_A^* \rangle^f}{\partial t^*} = \mathrm{D}_{eff}^* \frac{1}{r^*} \frac{\partial}{\partial r^*} \left(r^* \frac{\partial \langle c_A^* \rangle^f}{\partial r^*} \right) - Ki\, a_v^* \langle c_A^* \rangle^f \quad R_1^* \le r^* \le R_2^* \tag{8a}$$

$$\text{B.C.1} \quad \frac{\partial \langle c_A^* \rangle^f}{\partial r^*} = 0 \quad r^* = R_1^* \tag{8b}$$

$$\text{B.C.2} \quad \langle c_A^* \rangle^f = c_A^* \quad r^* = R_2^* \tag{8c}$$

$$\text{B.C.3} \quad \mathrm{D}_{eff}^* \frac{\partial \langle c_A^* \rangle^f}{\partial r^*} = \frac{\partial c_A^*}{\partial r^*} \quad r^* = R_2^* \tag{8d}$$

$$\frac{\partial c_A^*}{\partial t^*} = \frac{1}{r^*} \frac{\partial}{\partial r^*} \left(r^* \frac{\partial c_A^*}{\partial r^*} \right) \quad R_2^* \le r^* \le R_3^* \tag{8e}$$

$$\text{B.C.4} \quad c_A^* = 1 \quad r^* = R_3^* \tag{8f}$$

$$\text{I.C.1} \quad \langle c_A^* \rangle^f = c_A^* = 1 \quad t^* = 0 \tag{8g}$$

where *Ki* is the cell kinetic number defined by the ratio between the reaction rate and the diffusion rate at the scale of the unit cell

$$Ki = \frac{\ell_R}{\ell_p} Ki_p = k_0 \exp\left(\frac{-\alpha n F (E - E^0)}{RT} \right) \ell_R / D_A \tag{9}$$

and D_{eff}^* the normalized effective diffusion coefficient, $\mathrm{D}_{eff}^* = \varepsilon_f \mathrm{D}_{eff}/D_A$ with $\mathbf{D}_{eff} = \mathrm{D}_{eff}\mathbf{I}$ for isotropic structures. The software COMSOL Multiphysics was used to solve first the closure problem for **b** on a geometrical unit cell of the structure (see Figure 1) to obtain D_{eff} (here, $\mathrm{D}_{eff}^* = 0.376$) and then to solve the initial boundary value problem in Eqs. (8) for which the values of the physical parameters are reported in Table 1.

Table 1. Parameters used in the simulations.

Parameter	Symbol	Value	Unit
Ideal gas constant	R	8.314	J/(molK)
Faraday's constant	F	96485	C/mol
Number of electron transferred	n	2	–
Standard potential vs. $E_{Ag/AgCl}^0$	E_0	1.56	V
Temperature	T	298	K
Bulk concentration	c_A^0	10	mol/m^3
Diffusion coefficient	D_A	10^{-9}	m^2/s
Spherical pore diameter	$d_s = \ell_p$	1.17	μm
Pore connection window size	d_c	$0.15 d_s$	m
Size of the periodic unit cell	ℓ_R	1.64	μm
Porosity	ε_f	0.763	
Specific surface area	a_v	3.567×10^6	m^{-1}
Potential scan rate	r_E	0.5	mV/s

The current intensity can finally be computed according to Eq. (7), i.e.,

$$I = -n k_0 F \exp\left(\frac{-\alpha n F (E - E^0)}{RT} \right) \frac{S_{act}}{S} \int_S \langle c_A \rangle^f \mathrm{d}S \tag{10}$$

Experimental results of voltammetry obtained with the five electrodes are reported in Figure 2, together with results from the simulation of the above problem. It should be noted that the values of α and k_0 are not known a priori as they intimately depend on the pore coating material and surface texture as well as on the reaction under concern. For this reason, these two parameters were fitted, in the sense of the least square error, on the experimental curve obtained with the 11*HL* electrode, yielding $k_0 = 1.7 \times 10^{-17}$ cm/s and $\alpha = 0.482$. These values were further used for all the other electrode thicknesses. Moreover, the diffusion layer thickness, L_N, is also unknown. It depends on the electrode thickness and should be considered as time-dependent. For the sake of simplicity, a constant value for each electrode was adopted by fitting this parameter on each experimental curve, leading to $L_N = 800$ μm, 700 μm,

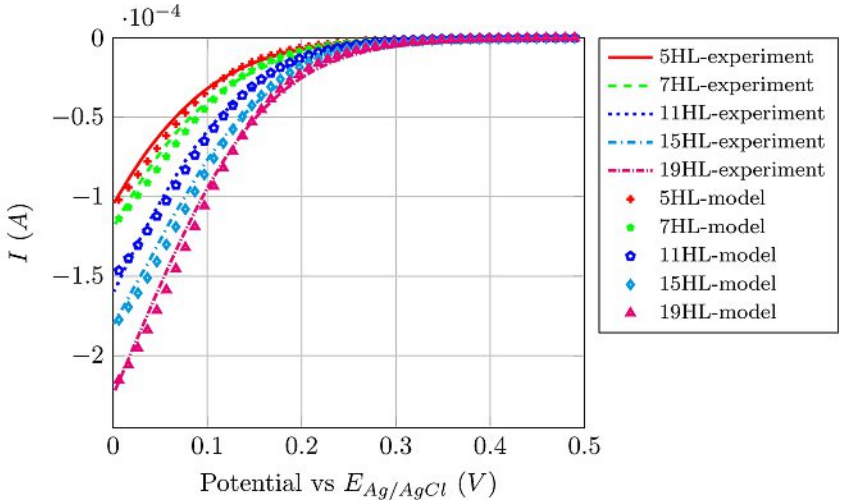

Figure 2. Intensity versus scanning potential obtained from voltammetry experiments performed with a potential scan rate $r_E = 0.5$ mV/s for the five electrodes. The solution is a 10 mM H_2O_2 in a 0.5 M H_2SO_4 at $T = 298$ K. Comparison with numerical simulations of the predictive macroscopic model (Eqs. (8)).

500 μm, 450 μm and 350 μm for the 5*HL*, 7*HL*, 11*HL*, 15*HL* and 19*HL* electrodes respectively. The relatively large values of L_N result from the low scan rate used in the experiments that are close to steday-state. Although the overall electron transfer involves two electrons, a pseudo elementary limiting step occurs with a single electron transfer. As a consequence, the exponential term in the Butler-Volmer equation is considered with $n = 1$.[24]

As can be observed in Figure 2, the agreement between the experimental data and numerical predictions is excellent. The maximum relative error between the two, over the whole range of potential and for all the electrodes, is less than 6.5 %, confirming the validity of the macroscale model.

In order to progress towards the determination of an optimal electrode thickness, it is important to evaluate the regime under which it is supposed to operate, as the optimum might differ whether the coupled transport-reaction process is unsteady or close to steady-state. In many applications, variations of the external parameters are slow enough for a steady approximation to be valid. For instance, the voltammetry experiments presented above can be accurately modelled using a steady version of the governing equations within the electrode and diffusion layer. This is confirmed by the current intensity versus the scanning potential represented in Figure 3a obtained from the unsteady model in Eqs. (8), on the one hand, and from its steady version in which the accumulation terms were neglected in Eqs. (8a) and (8e), on the other hand. As shown in Figure 3b, representing the maximum relative error on the current between the two approaches versus the potential scan rate for 19*HL* and the set of parameters of

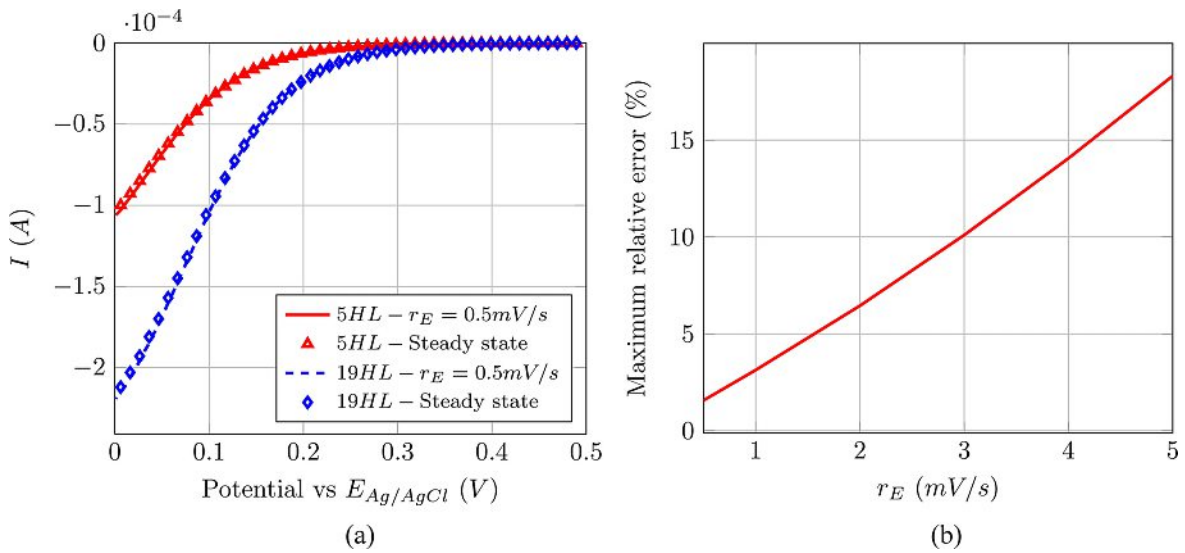

Figure 3. a) Current intensity versus scanning potential obtained from the complete unsteady model and its steady version for the 5*HL* and 19*HL* electrodes. b) Maximum relative error on the current intensity obtained with the unsteady and steady models for 19*HL* with a potential scan rate ranging from 0.5 mV/s to 5 mV/s over the potential interval [0, 0.5 V]. Parameters are those in Table 1.

Table 1, this maximum relative error remains smaller than 10% for r_E up to about 3 mV/s.

Under these circumstances, it seems relevant to determine the optimal thickness for operating conditions corresponding to the steady regime.

3.2. Steady-State Solution

The objective is to derive an analytical solution to the steady version of Eqs. (8) from which the optimal thickness of a cylindrical electrode can be determined. The solution to the steady version of Eqs. (8), referred to as the *full model* in the remainder of the article, involves Bessel series which are not easy to handle to carry out a complete analytical development. To circumvent this difficulty, an approximation can be used which consists in assuming that the ratio between the electrode thickness and its mean radius, $2L_e^*/\left(R_1^*+R_2^*\right)$, remains small compared to unity so that the electrode can be treated as a plane one. As a consequence, the mass conservation equation in the electrode can be written in cartesian coordinates, r^* denoting the dimensionless coordinate in the thickness direction, so that the two equations to be solved are

$$\frac{\mathrm{d}^2\left\langle c_A^*\right\rangle^f}{\mathrm{d}r^{*2}}=\varphi^2\left\langle c_A^*\right\rangle^f \quad R_1^*\le r^*\le R_2^* \tag{11a}$$

$$\frac{\mathrm{d}}{\mathrm{d}r^*}\left(r^*\frac{\mathrm{d}c_A^*}{\mathrm{d}r}\right)=0 \quad R_2^*\le r^*\le R_3^* \tag{11b}$$

together with the boundary conditions B.C.1 to B.C.4 in Eqs. (8b), (8c), (8d) and (8f). In Eq. (11a), φ is the cell Thiele modulus given by

$$\varphi=\sqrt{\frac{Ki\,a_v^*}{\mathrm{D}_{eff}^*}} \tag{12}$$

It must be noted that the radial coordinate is kept in the diffusion layer since the ratio $2L_N^*/\left(R_1^*+R_3^*\right)$ (i.e., the diffusion layer thickness to its mean radius ratio) is not small compared to unity in the general case. This yields a model, referred to as the hybrid model in the following, whose analytical solution is given by

$$\left\langle c_A^*\right\rangle^f=a\,\cosh\left(\varphi\left(r^*-R_1^*\right)\right) \quad R_1^*\le r^*\le R_2^* \tag{13a}$$

$$c_A^*=b\,\ln r^*+c \quad R_2^*\le r^*\le R_3^* \tag{13b}$$

with

$$a=\left(\mathrm{D}_{eff}^*\varphi\sinh\left(\varphi L_e^*\right)R_2^*\ln\left(R_3^*/R_2^*\right)+\cosh\left(\varphi L_e^*\right)\right)^{-1} \tag{14a}$$

$$b=\left(\frac{\coth\left(\varphi L_e^*\right)}{\mathrm{D}_{eff}^*R_2^*\varphi}+\ln\left(R_3^*/R_2^*\right)\right)^{-1} \tag{14b}$$

$$c=1-b\,\ln\left(R_3^*\right) \tag{14c}$$

Inserting Eq. (13a) into the expression of the current intensity in Eq. (7) yields

$$I=-\frac{nFD_AKi\,a_v^*V_e}{\ell_R^2L_e^*\left[Ki\,a_v^*R_2^*\ln(R_3^*/R_2^*)+\varphi\coth(\varphi L_e^*)\right]}c_A^0 \tag{15}$$

where V_e is the volume of the electrode immersed in the reactive solution.

To check the validity of the approximation made with the hybrid model, numerical simulations of the full model were performed with the software COMSOL Multiphysics. In Figure 4,

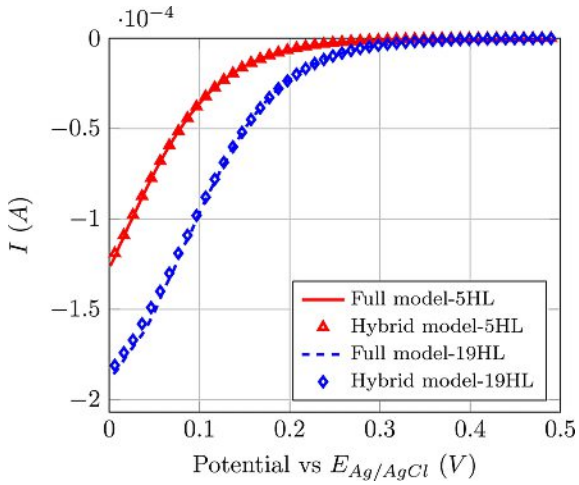

Figure 4. Current intensity versus the scanning potential obtained from the full and hybrid models for the 5*HL* and 19*HL* electrodes. $L_N=400$ µm.

results of the current intensity versus the scanning potential obtained from these simulations are compared to the analytical solution in Eq. (15) for the 5*HL* and 19*HL* electrodes, keeping the parameters reported in Table 1 and $L_N=400$ µm. This figure shows that the hybrid model provides a very accurate solution, the agreement with the full model being excellent. The largest discrepancy between the two models occurs for the smallest values of the potential and increases with the electrode thickness. Nevertheless, for the 19*HL* electrode, the maximum relative error is ~3.2%.

3.3. Optimal Electrode Thickness

The hybrid model is now employed to determine the optimal thickness of a cylindrical porous electrode. It must be noted that, at this stage, no special assumption is made on the type of microsctructure of the electrode material.

Although the magnitude of I monotonically increases with L_e^*, the electrode volume, V_e, increases much faster so that the volume current density, defined as the ratio $|I/V_e|$, tends to zero in the limit of infinite electrode thickness, justifying the determination of an optimal value of L_e^*, denoted L_e^{*op}. An example of the volume current density for a FCC structure representative of the electrodes used in the experiments

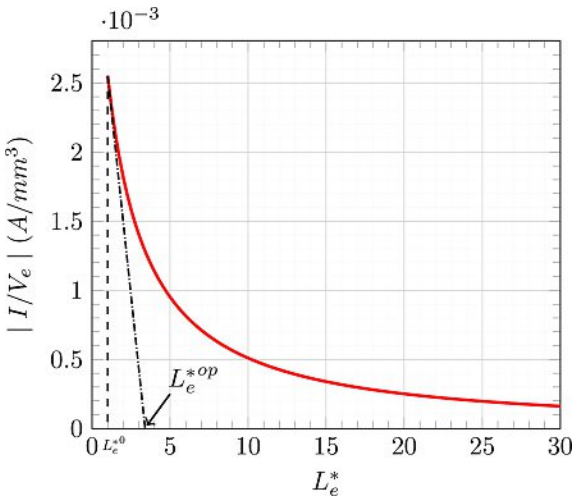

Figure 5. Variation of the volume current density, $|I/V_e|$, versus the electrode's dimensionless thickness, L_e^*, in the particular case of the FCC microstructure representing the material of the electrodes employed in the experiments. $Ki = 10^{-3}$, L_N=400 μm.

reported above is represented versus L_e^* in Figure 5 for a kinetic number $Ki = 10^{-3}$ and a diffusion layer thickness L_N=400 μm, all other parameters being those given in Table 1.

Typically, $|I/V_e|$ exhibits two asymptotic regimes, namely, a strong quasi-linear decrease at small value of L_e^* and, in the limit of very large values of L_e^*, a quasi-linear decrease to zero with a much smaller slope. As a result, the optimal thickness can be defined as the value at the crossover between these two asymptotic regimes, as schematically represented in Figure 5. More precisely, L_e^{*op} may be computed as the value of L_e^* at the intersecting point of the tangent to $|I/V_e(L_e^*)|$ at L_e^{*0} with $|I/V_e| = 0$. Here, L_e^{*0} should be taken as the minimum thickness that can be reasonably achieved experimentally, corresponding, for instance, to at least one unit cell, i.e., $L_e^{*0} \geq 1$.

In order to derive the analytical relationship providing L_e^{*op}, the expression of $\frac{\partial|I/V_e|}{\partial L_e^*}$ is required first. It is given by

$$\frac{\partial|I/V_e|}{\partial L_e^*} = -\frac{nFD_AKi\ a_v^*}{\ell_R^2 L_e^{*2}} \times \frac{\varphi^2 L_e^* + \varphi\coth(\varphi L_e^*) - \varphi^2 L_e^* \coth^2(\varphi L_e^*) + Ki\ a_v^* R_2^*\ \ln(R_3^*/R_2^*)}{\left(\varphi\coth(\varphi L_e^*) + Ki\ a_v^* R_2^*\ \ln(R_3^*/R_2^*)\right)^2} c_A^0 \tag{16}$$

This allows to express L_e^{*op} as

$$L_e^{*op} = -\frac{|I/V_e|_{L_e^{*0}}}{\frac{\partial|I/V_e|}{\partial L_e^*}_{|L_e^{*0}}} + L_e^{*0} = L_e^{*0}\left(\frac{\varphi\coth(\varphi L_e^{*0}) + Ki\ a_v^* R_2^* \ln(R_3^*/R_2^*)}{\varphi^2 L_e^{*0} + \varphi\coth(\varphi L_e^{*0}) - \varphi^2 L_e^{*0}\coth^2(\varphi L_e^{*0}) + Ki\ a_v^* R_2^* \ln\left(R_3^*/R_2^*\right)} + 1\right) \tag{17}$$

where $R_2^* = R_1^* + L_e^{*0}$ and $R_3^* = R_2^* + L_N^*$.

It must be noted that, for a given electrode structure (i.e., for fixed values of R_1^*, ℓ_R, a_v^* and D_{eff}^*), L_e^{*op} depends on Ki and L_N^*.

The optimization process may now be illustrated on the type of electrodes employed in the experiments reported above, i.e., assuming a FCC microstructure. In that case, a reasonable choice for L_e^{*0} is $L_e^{*0} = 1$, which corresponds to a minimum electrode thickness $(N_h = 4)$. Using this value, L_e^{*op} was computed from Eq. (17) and the resulting dependence of L_e^{*op} on the kinetic number for three values of the diffusion layer thickness, L_N, chosen in the range of those estimated from the experiments presented above, is reported in Figure 6. The

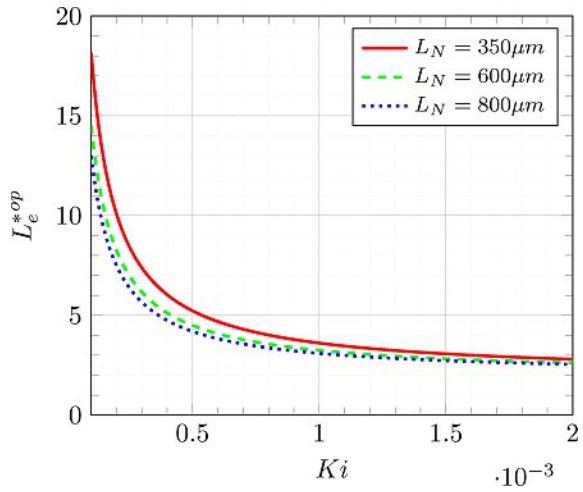

Figure 6. Optimal electrode thickness versus the kinetic number, Ki, for three values of L_N. Characteristics of the FCC structure are those indicated in Table 1. The corresponding optimal number of half layers is $4\,L_e^{*op}$.

optimal thickness varies significantly for very small values of the kinetic number and is quite insensitive to this parameter for $Ki \gtrsim 10^{-3}$. For Ki smaller than this value, L_e^{*op} also depends on the diffusion layer thickness characteristic of the configuration under concern. Almost no dependence on L_N is observed for $Ki \gtrsim 10^{-3}$. For the electrodes used in the H_2O_2/H_2O reduction experiments reported in Figure 2, Ki is approximately 1.54×10^{-7}, 8.40×10^{-5} and 1.54×10^{-3} when the potential takes the values 0.48 V, 0.1 V and 0 V respectively. This indicates that, if these electrodes are supposed to operate at a potential close to 0 V, the optimal thickness is about 12*HL*, whereas, for a potential of ~0.1 V, the optimal thickness is rather ~ 40*HL*. For a FCC microstructure, 4HL refers to 1 unit cell of size ℓ_R. If the dimensional characteristics are those given in Table 1, this means that 12*HL* and 40*HL* correspond to 4.92 μm and 16.4 μm respectively. Although operating conditions are quite different, it should be noted that these values are close to those reported in Cai et al.[25] (from 5 μm to 15 μm) for a plane solid oxide fuel cell.

To summarize, the optimization analysis shows that, in the general case, once the microstructural characteristics of the electrode material are carefully identified, the operating conditions must be cautiously specified as well in order to properly estimate the optimal thickness of the electrode. As a final important remark, it must be emphasized that the relationship in Eq. (17) should serve as a predictive tool to estimate the

optimal thickness of an electrode operating a single redox reaction in the steady regime, the thickness to mean radius ratio remaining small compared to unity. This predictive relationship is not restricted to any particular structure like the FCC used in Figure 6 for illustration purposes.

4. Conclusions

In this article, a multiscale model for the coupled diffusion-reaction process in porous electrodes proposed in a previous work[24] was validated with voltammetry experiments carried out on a series of electrodes operating an H_2O_2/H_2O reduction reaction. An analytical solution of this model was developed in the steady regime and for cylindrical electrodes featuring a small thickness to mean radius ratio compared to unity, both conditions being easily met in practice. This analytical model was further used to derive an analytical expression for the optimal electrode thickness which is general, regardless the internal porous structure of the electrode material, and this represents a net advantage over the analyses reported so far. From a practical point of view, the model requires the knowledge of the microsctructure in a representative elementary volume of the porous structure. This can be extracted from an image obtained on the real material or, as illustrated above, from a model structure that reproduces the essential geometrical features of the actual one. This optimal thickness is defined as the crossover value of two asymptotic regimes characterizing the volume current density dependence upon the electrode thickness, namely in the limit of extremely small and exceedingly large electrodes thicknesses respectively.

The analysis indicates that the optimal thickness does not only depend on the electrode internal radius and on the intrinsic parameters of the porous material, namely the size of the representative elementary volume of the microstructure, its specific area and macroscopic effective diffusion coefficient. It may also be sensitive to the operating conditions which can be reduced to two parameters: the kinetic number, *Ki*, and diffusion layer thickness developing at the outer boundary of the electrode. The optimal electrode thickness significantly depends on these two parameters in the range of very small values of *Ki*, but remains constant beyond a threshold value. For the electrodes and reaction under study in this work, this threshold corresponds to $Ki \sim 10^{-3}$, i.e., a potential of ~20 mV.

Acknowledgements

This work was supported by the LabEx AMADEus (ANR-10-LABX-42) within IdEx Bordeaux (ANR-10-IDEX-03-02), i.e., the "Investissements d'Avenir Programme" of the French government managed by the Agence Nationale de la Recherche (ANR). It also benefited from the support of the ANR projects MOMA (ANR-17-CE08-0005) and BIO3 (ANR-16-CE19-0001).

Conflict of Interest

The authors declare no conflict of interest.

Keywords: computational chemistry · optimization · porous electrodes · redox chemistry · volume averaging method

[1] D. Leech, P. Kavanagh, W. Schuhmann, *Electrochim. Acta.* **2012**, *84*, 223–234.
[2] T. Q. N. Do, M. Varničić, R. Hanke-Rauschenbach, T. Vidaković-Koch, K. Sundmacher, *Electrochim. Acta* **2014**, *137*, 616–626.
[3] T. Q. N. Do, M. Varničić, R. Flassig, T. Vidaković-Koch, K. Sundmacher, *Bioelectrochemistry* **2015**, *106*, 3–13.
[4] S. Cosnier, A. J. Gross, A. L. Goff, M. Holzinger, *J. Power Sources* **2016**, *325*, 252–263.
[5] M. Rasmussen, S. Abdellaoui, S. D. Minteer, *Biosens. Bioelectron.* **2016**, *76*, 91–102.
[6] S. Shleev, *ChemPlusChem* **2017**, *82*, 522–539.
[7] M. Gamella, A. Koushanpour, E. Katz, *Bioelectrochemistry* **2018**, *119*, 33-42.
[8] N. Mano, A. de Poulpiquet, *Chem. Rev.* **2018**, *118*, 2392–2468.
[9] S. Reculusa, M. Heim, F. Gao, N. Mano, S. Ravaine, A. Kuhn, *Adv. Funct. Mater.* **2011**, *21*, 691–698.
[10] A. Karajic, S. Reculusa, M. Heim, P. Garrigue, S. Ravaine, N. Mano, A. Kuhn, *Adv. Mater. Interfaces* **2015**, *2*, 1500192–1500196.
[11] A. Walcarius, A. Kuhn, *TrAC Trends Anal. Chem.* **2008**, *27*, 593–603.
[12] A. Karajić, S. Reculusa, S. Ravaine, N. Mano, A. Kuhn, *ChemElectroChem* **2016**, *3*, 2031–2035.
[13] R. Szamocki, S. Reculusa, S. Ravaine, P. N. Bartlett, A. Kuhn, R. Hempelmann, *Angew. Chem. Int. Ed.* **2006**, *45*, 1317–1321; *Angew. Chem.* **2006**, *118*, 1340–1344.
[14] R. D. Levie, *Adv. Electrochem. Electrochem. Eng.* **1967**, *6*, 329–397.
[15] O. E. Barcia, E. D'Elia, I. Frateur, O. R. Mattos, N. Pebere, B. Tribollet, *Electrochim. Acta* **2002**, *47*, 2109–2116.
[16] T. Vidaković-Koch, K. Sundmacher, In *Encyclopedia of Interfacial Chemistry* ; K. Wandelt, (Ed: Elsevier: Oxford), **2018**; pp 392–401.
[17] J. Galceran, S. L. Taylor, P. N. Bartlett, *J. Electroanal. Chem.* **2001**, *506*, 65–81.
[18] E. O. Barnes, X. Chen, P. Li, R. G. Compton, *J. Electroanal. Chem.* **2014**, *720–721*, 92–100.
[19] Z. Ban, E. Katelhon, R. G. Compton, *J. Electroanal. Chem.* **2016**, *776*, 25–33.
[20] H. T. H. Chan, E. Katelhon, R. G. Compton, *J. Electroanal. Chem.* **2017**, *799*, 126–133.
[21] B. Nam, R. T. Bonnecaze, *J. Electrochem. Soc.* **2017**, *154*, 191–197.
[22] R. T. Bonnecaze, N. Mano, B. Nam, A. Heller, *J. Electrochem. Soc.* **2007**, *154*, 44–47.
[23] P. D. Vidts, R. E. White, *J. Electrochem. Soc.* **1997**, *144*, 1343–1352.
[24] T. D. Le, D. Lasseux, X. P. Nguyen, G. L. Vignoles, N. Mano, A. Kuhn, *Chem. Eng. Sci.* **2017**, *173*, 153–167.
[25] Q. Cai, C. S. Adjiman, N. P. Brandon, *Electrochim. Acta* **2011**, *56*, 10809–10819.
[26] S. Whitaker, *The method of volume averaging*, 1st ed.; Kluwer Academic Publishers: Dordrecht, The Netherlands, **1999**.
[27] A. Fick, *J. Membr. Sci.* **1995**, *100*, 33–38.
[28] J. A. V. Butler, *Trans. Faraday Soc.* **1932**, *28*, 379–382.
[29] F. Valdés-Parada, D. Lasseux, S. Whitaker, *Int. J. Chem. React. Eng.* **2017**, *15*, 20170151.
[30] S. Reculusa, S. Ravaine, *Chem. Mater.* **2003**, *15*, 598–605.
[31] R. Szamocki, A. Velichko, F. Mücklich, S. Reculusa, S. Ravaine, S. Neugebauer, W. Schuhmann, R. Hempelmann, A. Kuhn, *Electrochem. Commun.* **2007**, *9*, 2121–2127.